Title
On the contact region of a diffusion-limited evaporating drop: a local analysis

Author
Morris, SJS

Publication Date
2014-01-25

DOI
10.1017/jfm.2013.577

Peer reviewed

On the contact region of a diffusion–limited evaporating drop: a local analysis

S. J. S. MORRIS †,

Department of Mechanical Engineering, University of California, Berkeley, CA 94720, USA

(Received 28 October 2013)

Motivated by experiments showing that a sessile drop of volatile perfectly–wetting liquid initially advances over the substrate, but then reverses, we formulate the problem describing the contact region at reversal. Assuming a separation of scales, so that the radial extent of this region is small compared with the instantaneous radius a of the apparent contact line, we show that the time scale characterizing the contact region is small compared with that on which the bulk drop is evolving. As a result, the contact region is governed by a boundary–value problem, rather than an initial–value problem: the contact region has no memory, and all its properties are determined by conditions at the instant of reversal. We conclude that the apparent contact angle θ is a function of the instantaneous drop radius a, as found in the experiments. We then non–dimensionalize the boundary–value problem, and find that its solution depends on one parameter $\mathcal{L}$, a dimensionless surface tension. According to this formulation, the apparent contact angle is well–defined: at the outer edge of the contact region, the film slope approaches a limit that is independent of the curvature of bulk drop. In this, it differs from the dynamic contact angle observed during spreading of non–volatile drops. Next, we analyse the boundary–value problem assuming $\mathcal{L}$ to be small. Though, for arbitrary $\mathcal{L}$, determining θ requires solving the steady diffusion equation for the vapour, there is, for small $\mathcal{L}$, a further separation of scales within the contact region. As a result, θ is now determined by solving an ordinary differential equation. We predict that θ varies as $a^{-1/6}$, as found experimentally for small drops ($a < 1$ mm). For these drops, predicted and measured angles agree to within 10–30%. Because the discrepancy increases with a, but $\mathcal{L}$ is a decreasing function of a, we infer that some process occurring outside the contact region is required to explain the observed behaviour of larger drops having $a > 1$ mm.

Key words:

1. Introduction

In recent experiments (Poulard et al. 2005; Guéna et al. 2007a,b), a sessile drop of pure liquid evaporates into a mixture of its own vapour and an inert gas at a rate controlled by vapour diffusion. The temperature T can be assumed uniform in space and time. The total gas pressure p_T is uniform; far from the drop, the partial pressure p_v approaches the constant $p_s - \Delta p_v$; p_s is the saturation pressure at temperature T, and $\Delta p_v \geqslant 0$. Though perfectly wetting, this system exhibits an apparent contact angle: θ is defined experimentally to be the slope measured at the inflexion point on the drop profile; it is a property of the small–scale flow induced by evaporation, and vanishes for $\Delta p_v = 0$. Under certain conditions, a drop spreads over the substrate until evaporation forces

† Email address for correspondence: morris@berkeley.edu

the apparent contact line to retreat. During reversal, the contact line is stationary; see figure 2.1 of Guéna (2007, p.35). (We note that, unlike a, the contact angle decreases monotonically over the drop lifetime: as shown by figure 2.10 of Guéna (2007, p.50), the decrease is rapid during spreading, but much slower during retreat.) Here, we treat only the stationary contact line.

Guéna et al (2007a, figures 6 and 3) show experimentally that, for a given liquid, θ and the drop radius a at reversal are each functions of initial drop volume v, even when v is varied 1000–fold. As shown in figure 11 of Guéna et al. (2007), eliminating v between those relations gives θ as a function of a. The absence of dependence on initial conditions suggests that θ is a property of the contact region at the instant of reversal, and is independent of the history of that region.

To interpret the θ–a relation, Poulard et al.(2005, equation 9) outline a model, referred to in their subsequent papers as the 'wedge model'. Assuming that the system is isothermal and that, within the contact region, the flow is quasi–steady, the authors use scaling to obtain a relation between θ and a. In essence, θ is assumed to form within a region having two defining properties: capillary pressure balances disjoining pressure and, at same scale, the divergence of the mass flux along the film balances the evaporative mass flux given by equation (5) of Deegan et al.(2000). According to equation (14) of Poulard et al. (2005), $\theta \propto a^{-1/6}$: because larger drops have a smaller gradient in chemical potential within the vapour, θ varies inversely with drop size. According to Guéna et al.(2007a, §6.1), for $a < 1$ mm (roughly), measured angles obey the one–sixth rule predicted by the wedge model.

For larger drops, a stronger dependence on a is observed. Cazabat (pers. comm.) has pointed out that for these drops, buoyant convection within the gas is likely to affect mass transfer at the drop scale. Kelly–Zion et al. (2013) report measured values of evaporation rates from sessile drops of a liquid whose vapour phase is denser than air; the contact line was pinned. Comparing their figures 3 and 4, we see that for a heptane droplet with $a = 8$ mm, the evaporation rate is about 3 times that expected from pure diffusion. Because, at the scale of the whole drop, buoyant convection influences the mass transfer, it is useful to separate the problem of determining θ from that of the large–scale dynamics.

Here, we formulate and analyse the boundary–value problem defining the contact region. Our formulation is *local* in the sense that we exploit the separation of length scales existing between this small region, and the macroscopic drop: the radial dimension of the contact region is small compared with the radius a of the apparent contact line. We make the following assumptions. (a) Within the gas, mass transfer occurs by steady diffusion, even when buoyant convection is significant at the drop scale. This is a good approximation provided the Péclet number based on the dimension of the contact region is small compared with unity. (b) The system is isothermal; for the Guéna experiments this assumption is justified because the thermal conductivity of the silicon substrate is three decades larger than that of the liquid. (c) Within the contact region, the liquid motion is quasi–steady: at each instant, the divergence of the radial mass flux balances the evaporative mass flux into the gas. This is subsequently shown to be a good approximation whenever there is a separation of length scales. (d) Because, in the experiments, $\theta \ll 1$, boundary conditions on the liquid–gas interface are transferred onto the plane $y = 0$. (For brevity, we continue to call these the 'interfacial' conditions, even after their transfer to $y = 0$.)

Together, assumptions (a) to (d) allow us to replace the initial–value problem governing the whole drop by a boundary–value problem; the contact angle and distribution of evaporative mass flux are determined by the solution of this problem. To complete its

formulation, the partial pressure p_v of vapour must be imposed as a outer boundary condition holding on a large semi–circular arc bounding the contact region.

This outer condition is not arbitrary. Far from the apparent contact line, the interfacial conditions simplify. Towards the macroscopic drop, they require p_v to approach the saturation pressure appropriate to the system temperature; towards the molecular scale wetting film, they require the evaporative mass flux to vanish. Together with the Laplace equation for p_v, these conditions constrain the variation of p_v along the perimeter of the semicircle bounding the contact region. By separation of variables, we find that p_v must be expressible as a superposition of certain basis functions. Matching to an outer solution, specific to the mass transfer process at the drop scale, requires p_v to take the form of one of these basis functions. The drop–scale transport process selects that function, and determines its amplitude.

To illustrate our formulation, we work out the details for a drop sufficiently small for mass transfer to be by pure diffusion, even at the scale of the whole drop. In §2, the boundary–value problem is stated without derivation, but with the underlying assumptions identified. In §3, the problem is non–dimensionalized. With the scales in hand, in §4 the underlying assumptions are shown to hold provided the radial scale of the contact region is small compared with the radius a of the apparent contact line; this is also the condition under which the notion of an apparent contact line has meaning.

The boundary–value problem contains one parameter: $\mathcal{L}$ is a dimensionless surface tension and is a decreasing function of a. In §5 the solution of the boundary–value problem is analysed in the limit as $\mathcal{L} \to 0$; the corresponding expression for θ is given in §6. Because this expression corresponds to a physical picture of the contact region, in §7 scaling is used to summarize that picture. In §8, we compare predicted and experimentally values of both the angle and the film thickness at which it is formed. There, we also discuss carefully the relation between the the theory and the observations. In §9, we summarize the main points of the paper, and we discuss the relation between our asymptotic analysis for small $\mathcal{L}$ and an approximation made by Eggers & Pismen (2010) in their a numerical simulation of an evaporating sessile drop.

In this work, the swung dash $\sim$ denotes an asymptotic relation: in a specified limit, $a \sim b \Leftrightarrow a/b \to 1$. The symbol $\approx$ is used where scaling arguments are used for interpretation.

2. Formulation

Figure 1 shows the geometry of the problem. The origin O is at the apparent contact line defined by extrapolating the tangent from infinity. Subscripts l, v denote the liquid and vapour phases. The unknowns are the vapour partial pressure p_v, liquid pressure p_l and film thickness h. The droplet planform radius a is assumed large compared with the radial dimension ℓ_0 of the contact region. This allows us to assume plane flow within the contact region.

In the experiments, θ is small (less than 0.08), allowing the use of lubrication theory to describe the liquid film. The liquid and vapour flows are coupled through the usual interfacial conditions. Because the drop is thin and the solution $p_v(x, y)$ of the Laplace equation varies on the radial length scale ℓ_0, boundary conditions on the vapour can be transferred from $y = h$ to $y = 0$ with error vanishing with the ratio h_0/ℓ_0 of characteristic film thickness h_0 to ℓ_0. By contrast, for the flow *within* the thin liquid film, the length scale in y is the thickness scale h_0. Consequently, boundary conditions on the liquid flow can not be transferred from $y = h$ to $y = 0$; instead lubrication theory must be used to account for the internal structure of the film. As a result, the unknowns p_v, p_l and h are

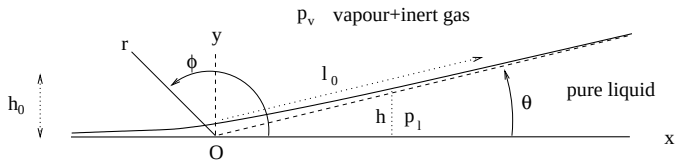

FIGURE 1. Contact region: scales h_0 and ℓ_0 are defined by (7).

determined by solving the Laplace equation for p_v in the half space $y > 0$, subject to boundary conditions on $y = 0$.

2.1. *Governing equations*

These are stated, then interpreted. The unknowns $p_l(x)$, $p_v(x, y)$ and $h(x)$ satisfy the following problem. For $y > 0$, and $-\infty < x < \infty$,

$$\nabla^2 p_v = 0. \tag{1a}$$

On $y = 0$

$$p_v - p_s = \frac{\rho_s}{\rho_l}(p_l - p_T), \tag{1b}$$

$$p_T - p_l = \gamma \frac{\mathrm{d}^2 h}{\mathrm{d}x^2} + \frac{A}{h^3}, \tag{1c}$$

$$0 = \frac{1}{3\nu_l}\frac{\partial}{\partial x}\Big[h^3 \frac{\partial p_l}{\partial x}\Big] + \frac{D_v}{R_v T}\frac{\partial p_v}{\partial y}. \tag{1d}$$

The conditions on h are

$$\lim_{x\to-\infty} h = 0, \quad \lim_{x\to\infty} \frac{\mathrm{d}h}{\mathrm{d}x} = \theta, \tag{1e,f}$$

where θ is to be determined as part of the solution. In these equations, the parameters are vapour diffusivity D_v, surface tension γ, dispersion constant A, the kinematic viscosity ν_l and density ρ_l of the liquid, saturation pressure p_s, saturation vapour density ρ_s, and the ratio R_v of the molar gas constant to vapour molar mass M. The temperature T is uniform in space and time. Material properties are given in Appendix B.

According to (1b), at each point on the interface, the partial pressure p_v of vapour is related to the pressure p_l on the liquid side by the linearized Gibbs–Thomson relation (Gibbs 1876, equation 287; Thomson 1872). For (1b) to hold, it is necessary that the liquid and its vapour be in *local* thermodynamic equlibrium across their interface; that being so, the local values of p_l and p_v are related by the nonlinear Gibbs–Thomson relation. That expression can be linearized for our purpose because, within the region of interest, the change in vapour density ρ_v proves to be small compared with the saturation vapour density ρ_s. (This statement is justified in §4.)

Local thermodynamic equilibrium is assumed without explanation by Doumenc and Guerrier (2010, equation 13) and by Eggers and Pismen (2010, equation 4). By scaling the interfacial mass balance, Njante (2012, Appendix A) shows that if the system is effectively isothermal, so that evaporation is diffusion–limited, the liquid and its vapour are in local equilibrium whenever the continuum approximation holds in the gas.

According to the Laplace–Young equation (1c), the difference between the total pressure p_T in the gas, and the liquid pressure p_l balances the resultant of the forces exerted by surface tension, and Van der Waals forces. For the latter ('disjoining pressure') we use the form appropriate to the non–retarded potential for non–polar molecules. Levinson et al. (1993, figure 3) show experimentally that for an octane film on oxidized silicon,

disjoining pressure varies as h^{-3} for film thicknesses lying (roughly) in the range 1–3 nm; see also Truong and Wayner (1987, figure 6). We return to this assumption at the end of §8.

The Reynolds equation (1d) expresses the film mass balance for quasi–steady flow: it has been assumed that there is no slip at the wall, and that the shear stress vanishes at the gas–liquid interface. For the latter condition to hold, surface tension γ must be uniform: Guéna (2007, pp.83–84) discusses the precautions taken to realize this condition in his experiments.

Although, to describe the evolution of the whole droplet, we would need to augment the Reynolds equation (1d) by adding the appropriate unsteady term, that term is negligibly small within the contact region. There, the gradient terms displayed in (1d) are large, whereas the magnitude of the unsteady term is determined by the slow evolution of the whole droplet. Section 4 contains a more detailed discussion.

Growth condition (1e) states that within the region described by problem (1), the film thickness is large compared with that characterizing the wetting film to the left of the origin in figure 1. This is a good approximation for the Guéna experiments in which the partial pressure vanishes far from the drop: because a liquid film can not coexist with a vacuum, the thickness of the wetting film then vanishes far from the drop. Lastly, in (1f), θ is to be determined as part of the solution.

Using (1b), we express (1c) and (1d) in terms of p_v: on $y = 0$,

$$\frac{\rho_l}{\rho_s}(p_s - p_v) = \gamma \frac{\mathrm{d}^2 h}{\mathrm{d}x^2} + \frac{A}{h^3}, \tag{1c$'$}$$

$$0 = \frac{\partial}{\partial x}\Big[h^3 \frac{\partial p_v}{\partial x}\Big] + 3L^2 \frac{\partial p_v}{\partial y}. \tag{1d$'$}$$

The Reynolds length L, defined by

$$L^2 = \frac{\rho_s \nu_l D_v}{\rho_l R_v T}, \tag{2}$$

is the dimension at which the two terms in (1d$'$) would balance if x, y and h were all comparable. Using the material properties given in Appendix B, we find that for the fluids used by Guéna et al. (2007a), $\gamma L^2/A$ takes the following values: 0.19 (nonane), 0.37 (octamethyltrisiloxane OMTS), 0.49 (octane) and 1.55 (hexamethyldisiloxane HMDS).

2.2. *Outer boundary condition*

To complete the formulation, we must prescribe p_v on a semicircle of radius $R \gg \ell_0$; in its present form, (1) is incomplete because it contains no information about the potential difference Δp_v driving evaporation.

This matching condition must be compatible with growth conditions (1e) and (1f); it must also be compatible with the solution of the outer (Deegan et al.) problem. Unlike the boundary–value being formulated here, that Deegan problem accounts for overall drop geometry, but does not describe the structure of the contact region itself.

We first consider the implications of the growth conditions. Because the volume flow along the film is proportional to h^3, we assume and then verify (equation 17), that the first condition (1e) requires the volume flow to vanish as $h \to 0$. The Reynolds equation (1d$'$) then requires that

$$\lim_{x \to -\infty} \frac{\partial p_v}{\partial y}\Big|_{y=0} = 0. \tag{3a}$$

Similarly, the second condition (1f) and the Laplace–Young condition (1c$'$) together

require that

$$\lim_{x\to\infty}(p_v - p_s)\big|_{y=0} = 0. \tag{3b}$$

In the first instance, (3a) and (3b) hold on the gas–liquid interface; they are, however, transferred to $y = 0$ using the argument given in §2, ¶2.

We digress to note that (3a) and (3b) are obtained by taking the outer limit of boundary conditions holding throughout the contact region. In their interpretation, (3a) and (3b) differ from similar conditions imposed by Deegan et al. on the outer problem, that is, their diffusion model of mass transfer at the drop scale. Viewed at that scale, the droplet has a triple junction at which all 3 components are in contact. On the gas–solid interface, a no–flux condition is applied, whereas on the gas–liquid interface, $p_v = p_s$; each condition is applied at all points on the appropriate interface. By contrast, because our inner problem resolves the structure of the contact region, no more than 2 components are ever in contact. Consequently, there is no triple junction, and conditions (3a), (3b) apply only in the limits stated.

Returning to the main argument, we use (3) to determine the most general form which the solution of (1) *could* take far from the apparent contact line. Because this form must be consistent with the growth conditions (1e) and (1f), it must satisfy the outer limit (3) of the boundary conditions (1c′) and (1d′), rather than the full conditions. By separation of variables, the general solution of the b.v.p. comprising (1a), (3a) and (3b) is a linear combination of basis functions

$$p_n = r^{n+1/2}\sin(n+\tfrac{1}{2})\phi, \tag{4}$$

(integer n). To interpret these modes, we note two properties. First, although $\partial p_0/\partial r > 0$ for $0 < \phi < \pi$, for $n \geqslant 1$, $\partial p_n/\partial r$ changes sign; whereas the zeroth mode represents a mass flow that would be outward at each point (for evaporation), higher modes permit inflow and might be expected to occur in systems in which condensation occurs at some points on the film. Second, for each n, $\int_0^\pi (\partial p/\partial r)\, r\mathrm{d}\phi \neq 0$; though higher order modes describe both outflow and inflow, each mode contributes to the radial mass flow. This determines the outer limit of the inner solution.

For sufficiently small droplets, mass transport at the scale of the whole drop occurs by steady diffusion. In this case, the distribution of vapour pressure *outside* the contact region is given by the b.v.p. posed by Deegan et al.(2000, equation 4). In the limit as $\theta \to 0$, the solution of that outer problem is given by the Weber formula (Landau–Lifshitz 1960, p.27; Cazabat and Guéna 2010. Appendix 1). Consequently, the Weber solution can be used to determine the outer boundary condition for the inner problem (1) determining θ, even though the Weber solution itself is independent of θ.

According to Landau–Lifshitz (1960, p.27), for $r \ll a$, the Weber formula simplifies to

$$p_v - p_s \sim -k\Delta p_v\sqrt{\frac{r}{a}}\sin\frac{\phi}{2}, \tag{5a}$$

$$k = 2\sqrt{2}/\pi. \tag{5b}$$

Comparing (5) with the pressure modes p_n defined by (4), we see that the solution of the inner problem (1) will match to the outer (Weber) solution provided (1) is solved subject to the outer boundary condition defined by (5). This completes the formulation.

When buoyant convection is significant at the drop scale, the numerical constant k must replaced by a function of the parameters controlling the convective motion. Depending on the transport process operating at the drop scale, another member of the family (4) might also be selected; I have not investigated this.

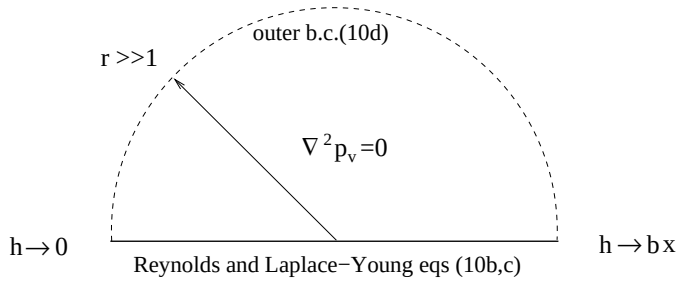

FIGURE 2. Summary of problem (10) defining the contact region.

3. Dimensionless boundary–value problem

3.1. *Definition of h_0 and ℓ_0*

These scales have two defining properties. In the Reynolds equation (1d′), the terms balance; in the Laplace–Young equation (1c′), the left hand side balances the second term on the right:

$$\frac{h_0^3}{\ell_0} = L^2, \qquad k\frac{\rho_l}{\rho_s}\Delta p_v \sqrt{\frac{\ell_0}{a}} = \frac{A}{h_0^3}. \tag{6a,b}$$

Eliminating h_0 between (6a) and (6b), we obtain

$$\ell_0 = a^{1/3} d^{2/3}/k^{2/3}; \;\; h_0 = L^{2/3} a^{1/9} d^{2/9}/k^{2/9}. \tag{7a,b}$$

The disjoining–diffusion length d is defined by

$$d = \frac{A}{\nu_l D_v \Delta\rho_v}; \tag{8}$$

on this scale, disjoining pressure balances the shear stress due to a volume flow $D_v\Delta\rho_v/\rho_l$. The notion of an apparent contact line is valid provided $\ell_0 \ll a$; according to (7), this separation of scales exists provided $a \gg d$.

Using the material properties given in Appendix B, we find that for the fluids used in the Guéna experiments d ranges from 0.9 nm (HMDS) to 9 nm (nonane). We note that d, h_0 and ℓ_0 are independent of γ.

We define dimensionless variables (without asterisks):

$$\{x, y\}^* = \ell_0\{x, y\}, \;\; h^* = h_0 h, \tag{9a,b}$$

$$p_v^* - p_s = k\,\Delta p_v \sqrt{\frac{\ell_0}{a}}\, p. \tag{9c}$$

Substituting (9) into (1) and (5), we find that for $y > 0$ and $-\infty < x < \infty$,

$$\nabla^2 p = 0. \tag{10a}$$

On $y = 0$

$$-p = \mathcal{L}\frac{\mathrm{d}^2 h}{\mathrm{d}x^2} + h^{-3}, \tag{10b}$$

$$0 = \frac{\partial}{\partial x}\Big[h^3\frac{\partial p}{\partial x}\Big] + 3\frac{\partial p}{\partial y}. \tag{10c}$$

As $r \to \infty$,

$$p \sim -\sqrt{r} \sin \frac{\phi}{2}. \tag{10d}$$

The conditions on $h(x)$ are

$$\lim_{x \to -\infty} h = 0, \qquad \lim_{x \to \infty} \frac{\mathrm{d}h}{\mathrm{d}x} = b. \tag{10e, f}$$

In (10f), the constant $b > 0$ is to be determined as part of the solution. In (10b), $\mathcal{L} = \gamma h_0^4/(A\ell_0^2)$; eliminating h_0^3/ℓ_0 between this definition and (6a), we find that

$$\mathcal{L} = \frac{\gamma L^2}{A}\theta_0, \tag{11}$$

$\theta_0 = h_0/\ell_0$. Because each of h_0, ℓ_0 and L is independent of γ, $\mathcal{L}$ is proportional to γ; it is a dimensionless surface tension.

Figure 2 summarizes the boundary–value problem. We note that the Weber solution enters (10) only as the outer boundary condition on the semi–circle of radius $R \gg \ell_0$ bounding the contact region. The evaporative flux from the liquid film is to be determined as part of the solution of (10); it is *not* obtained from the Weber formula.

This ends the statement of the boundary–value problem. As to its mathematical nature, we note that if h were given, (10a), (10b) and the outer boundary condition (10d) would define a Poisson problem for p. The solution of that Poisson problem prescribes the distribution flux $\partial p/\partial y$ along the x–axis. The function $h(x)$ is to be chosen to make this distribution compatible with the remaining condition (10c); this could, of course, be done by adding the appropriate unsteady term to the Reynolds equation, and solving (10) as an initial–value problem.

The contact angle is given by

$$\theta = \theta_0\, b(\mathcal{L}); \tag{12a}$$

$$\theta_0 = \frac{k^{4/9} L^{2/3}}{a^{2/9} d^{4/9}}. \tag{12b}$$

Equations (7a) and (7b) have been used. Because the unit of slope θ_0 is independent of γ, the contact angle depends on surface tension only through the slope parameter b.

Though the solution of (10) depends on the single parameter $\mathcal{L}$, the contact angle itself depends on two parameters θ_0 and $\mathcal{L}$. By (11), the magnitude of $\mathcal{L}$ is determined by that of θ_0, because $\gamma L^2/A$ is at most of the order of unity. Consequently, whenever the assumption $\theta \ll 1$ holds, the parameter $\mathcal{L}$ is also small. This fact is exploited in §5.

We note that θ_0 and $\mathcal{L}$ vary respectively as $A^{-4/9}$ and as $A^{-13/9}$, and A is not known precisely. According to Gee et al. (1989, figure 6), for the alkanes on silica A is known to within a factor of about 2; similarly, Levinson et al. (1993, p.484) find that the value of A measured for an octane film on silica agrees to within a factor of 2 with that predicted by Lifshitz theory. As a result of this uncertainty in a material property, the numerical values of θ_0 and $\mathcal{L}$ are themselves uncertain, for a reason entirely separate from the problem of the evaporating drop. Moreover, for the conditions of the Guéna experiments, we find in §6 that θ in fact depends only weakly on A. Because this uncertainty in material properties would swamp the relation being tested, it would be nugatory to try using (12) in the form of the similarity principle $\theta/\theta_0 = b(\mathcal{L})$. In this case, solving the boundary–value problem provides a result that no amount of dimensional analysis can approach.

Table 1 collects the chief parameters of the theory.

Reynolds length Eq.2	disjoining–diffusion length, Eq.8	slope unit Eq.12	Laplace parameter Eq.11	Density parameter Eq.48
$L = \left[\dfrac{\rho_s \nu_l D_v}{\rho_l R_v T}\right]^{1/2}$	$d = \dfrac{A}{\nu_l D_v \Delta\rho_v}$	$\theta_0 = \dfrac{L^{2/3} k^{4/9}}{a^{2/9} d^{4/9}}$	$\mathcal{L} = \dfrac{\gamma L^2}{A}\theta_0$	$\mathcal{D} = \dfrac{\nu_l D_v \Delta\rho_v}{(\gamma^3 A a^2)^{1/4}}$

TABLE 1. Chief parameters. As defined by (5b), $k = 2\sqrt{2}/\pi, = 0.900\ldots$, provided mass transfer at the drop scale is by pure diffusion.

4. Discussion of assumptions

4.1. *Linearized Gibbs–Thomson relation*

In our problem, a pure incompressible liquid is in contact with a perfect gas mixture comprising inert components and the vapour phase of the liquid. According to Gibbs (1875, equation 285), when the liquid pressure is increased by an amount $\mathrm{d}p_l$, the liquid and its vapour phase will remain in thermodynamic equilibrium if the partial pressure of vapour is increased by an amount $\mathrm{d}p_v$ given by $\mathrm{d}\ln p_v = \mathrm{d}p_l/(\rho_l R_v T)$.

As reference state, we use the condition holding on the interface as $x \to \infty$ in figure 1. There, p_l is equal to the total pressure p_T in the gas, and the liquid and its vapour coexist in equilibrium at partial pressure p_s. Integrating from this state to the thermodynamic state in which the liquid pressure is p_l, we obtain

$$p_l - p_T = \rho_l R_v T \ln \frac{p_v}{p_s}. \tag{13}$$

The total pressure p_T has been assumed to be uniform; in the experiments, this is a good approximation because the partial pressure is at most about 1% of the total pressure.

As (1b), we have used the linearized form of (13). This approximation is valid provided the change in p_v along the interface is small compared with p_s. In the Guéna experiments, this is not true for the whole drop because $\Delta p_v = p_s$: at the interface, p_v varies from p_s on the bulk drop to zero above the wetting film far from the bulk drop. Even in those experiments, however, the linearization is valid for the local formulation because the contact region does not see the entire variation in p_v. According to the outer boundary condition (5), within the contact region, p_v varies by an amount of the order of $\Delta p_v \sqrt{\ell_0/a}$. Even for $\Delta p_v = p_s$, this scale is small compared with p_s because $\ell_0 \ll a$.

We conclude that when the notion of an apparent contact line is applicable, the linearized Gibbs–Thomson relation (1b) holds within the contact region. Outside that region, we must use (13), however. In the Guéna experiments, for example, $p_v \to 0$ in the laboratory far from the drop; uncritically using (1b) to determine the wetting film thickness far from the bulk drop would then lead to the false conclusion that a liquid layer of finite thickness coexists with a vacuum.

4.2. *Separation of timescales*

As noted below (8), the notion of an apparent contact line is appropriate provided $a \gg d$, the disjoining–diffusion length. We now verify that this separation of spatial scales implies a separation of time scales: within the small contact region, the flow evolves on a time scale short compared with that on which the drop evolves as a whole. This is why there is no time derivative in the Reynolds equation (1d) describing the contact region. This separation of time scales is commonly assumed without explanation: see, for example, Bonn et al. (2009, equations 49, 64); Eggers and Pismen (2010, equation 39). However,

as we have discussed in §1, the behaviour of drops having Bond number $\rho_l g a^2/\gamma > 1$ is not understood. For this reason, we verify this approximation carefully.

Relative to axes fixed in the laboratory, and with the unsteady term included, the (dimensional) Reynolds equation for the whole drop is

$$\rho_l \frac{\partial h}{\partial t} = \frac{1}{3\nu_l\, s}\frac{\partial}{\partial s}\Big[sh^3\frac{\partial p_l}{\partial s}\Big] + D_v\frac{\partial \rho_v}{\partial y}; \tag{14}$$

s denotes radial distance from the symmetry axis of the drop. The ideal gas law $p_v = \rho_v R_v T$ has been used.

Balancing the left side of (14) against the second term on the right hand side, we find that, for the contact region, the time scale is given by $t_c = \rho_l h_0 (a\ell_0)^{1/2}/(kD_v\Delta\rho_v)$. (We have used the scales defined by (9).)

The drop as a whole, however, evolves on the longer time scale t_b set by the integral mass balance. To obtain that balance, we assume that, within the liquid film, the radial mass flow vanishes at the apparent contact line. This is a good approximation because, whenever the notion of an apparent contact line is applicable, the mass loss from the wetting film is negligibly small compared with that from the bulk drop. (For this, see the discussion below (26) and, again, below (50).)

Multiplying (14) by $2\pi s$, then integrating from $s = 0$ to a, we obtain the integral mass balance (Guéna et al. 2007a, equation 3):

$$2\pi\rho_l \int_0^a \frac{\partial h}{\partial t}\, s\,\mathrm{d}s = -4D_v a\Delta\rho_v.$$

To evaluate the diffusive flux, we have used results for the Weber solution given by Cazabat and Guéna (2010, Appendix 1). In using those results, we have assumed that, at reversal, the drop is shallow: its maximum height h_m is small compared with a. We have made no other assumption about drop shape, however. Because, for the drop as a whole, $\partial h/\partial t$ scales as the ratio of h_m to the time scale t_b, we conclude that $t_b = ah_{\mathrm{m}}\rho_l/(D_v\Delta\rho_v)$.

The ratio of time scales is given by $t_b/t_c = kh_{\mathrm{m}}a^{1/2}/(h_0\ell_0^{1/2})$. Provided $h_m \gg h_0$ and $a \gg \ell_0$, the bulk drop evolves on a time scale large compared with that of the contact region: $t_b \gg t_c$. This conclusion is independent of drop shape.

4.3. *Self–consistency of the outer boundary conditions (3)*

4.3.1. *Tapered film: equation(3a)*

We consider the behaviour as $r \to \infty$ within the tapered film to the left of the origin O in figure 1. Setting $\phi = \pi$ in (10d), we find that as $r \to \infty$

$$p \sim -\sqrt{r}. \tag{15}$$

To calculate the corresponding asymptote for h, we note that within the tapered film, the capillary pressure becomes negligibly small compared with the disjoining pressure. Using this observation to simplify the Laplace–Young condition (10b), we find that as $r \to \infty$

$$h \sim r^{-1/6} \tag{16}$$

the film thickness vanishes asymptotically within the tapered film. This is, of course, consistent with the first growth condition (10d) on h.

It remains to verify that the flux from the tapered film vanishes asymptotically as $h \to 0$. Using (15) and (16) to calculate the film transport (first term in the Reynolds

equation 10c), we find that

$$\frac{\partial}{\partial x}\Big[h^3\frac{\partial p}{\partial x}\Big] \sim \frac{\partial^2}{\partial r^2}(\ln h^3), \sim \frac{1}{2r^2}. \tag{17}$$

The Reynolds equation then requires that

$$\lim_{x\to-\infty}\frac{\partial p}{\partial y}\Big|_{y=0} = 0, \tag{18}$$

as stated by (3a).

4.3.2. *Wedge: equation (3b)*

We consider the behaviour as $x \to \infty$ on the interface separating the liquid wedge from the gas: as discussed above (4), as far the vapour is concerned, this interface is at $\phi = 0$. Using (9e) to evaluate the vapour flux at the interface, we obtain $\partial p/\partial y \sim -1/(2\sqrt{x})$. Substituting this expression into the Reynolds equation (10c), then integrating, we obtain

$$h^3\frac{\partial p}{\partial x} \sim 3\sqrt{x} + c_0. \tag{19}$$

The integration constant c_0 depends on $\mathcal{L}$.

For p to approach a constant on the interface, $\partial p/\partial x$ must be integrable at infinity; this is so if h grows more rapidly than $\sqrt{x}$. But, although existence of an apparent contact angle is, therefore, sufficient for $\partial p/\partial x$ to be integrable at infinity, it is not necessary. For example, in §5, we find that in the limit as $\mathcal{L} \to 0$, (10) has an inner–and–outer structure. At the outer edge of the inner region, h then grows more rapidly than x and, we find that although the contact angle has not yet formed, this rapid growth of h has already forced p to vanish on the interface.

For the moment, we need the simplest example showing that (3b) is consistent, and that (10) can define a contact angle. For this purpose, we assume, then verify, that an apparent contact angle has been formed, so that $h \sim bx$. Using this to solve (19) for p, we obtain

$$p(x,0) \sim -2/(b\sqrt{x})^3 : \quad \lim_{x\to\infty} p = 0, \tag{20a,b}$$

consistent with (3b).

To complete the example, we verify that the assumption $h \sim bx$ is self–consistent. Substituting (20a) into Laplace–Young equation (10b), then integrating in x, we find that as $x \to \infty$ ($\mathcal{L}$ fixed)

$$\frac{\mathrm{d}h}{\mathrm{d}x} \sim b - 4/(b^3\sqrt{x}). \tag{21}$$

Because $\mathrm{d}h/\mathrm{d}x$ approaches a limit as $x \to \infty$, an apparent contact angle has formed. We conclude that the formulation of (10) is self–consistent whenever the notion of an apparent contact line is applicable.

5. Analysis for small Laplace parameter $\mathcal{L} \to 0$

5.1. *The picture to be developed*

Figure 3 shows the contact region, as seen at two different scales. Figure 3a shows the axisymmetric bulk droplet with its precursor film. As stated in §1, far from the drop the dimensional partial pressure approaches the constant value $p_s - \Delta p_v$ in the free air in the laboratory. Because the pressure scale adopted in (9c) is asymptotically $o\big(\Delta p_v\big)$, the corresponding dimensionless pressure is large in magnitude and (of course) negative.

The precursor film is therefore asymptotically thin compared with the film thickness h_0 characterizing the contact region, now defined as the solution of (10). In figure 3a, this region is indicated by the broken rectangle.

Figure 3b shows the inner–and–outer structure of the contact region existing in the limit as $\mathcal{L} \to 0$. Because this structure is controlled by the thin liquid film, the film is described first. The *inner* region is defined by taking the limit as $\mathcal{L} \to 0$ (h fixed); it contains a slender tapered film. Though, within this region, the capillary pressure is negligibly small, film curvature proves to increase with increasing h, whereas the disjoining pressure falls. Consequently, for any small but fixed value of $\mathcal{L}$, the capillary pressure ultimately balances the disjoining pressure. Because $\mathcal{L}$ is small, this balance is possible only when the film attains a thickness $O(h_1)$ which is asymptotically large in $\mathcal{L}$. The corresponding scales h_1 and ℓ_1 are defined quantitatively by (31). The scale h_1 locates the *corner*, shown as region *abcd* in figure 3b. (Though h_1 is large, the film, of course, remains slender because $h_0 \ll \ell_0$.) The contact angle is formed within the corner.

Because the disjoining pressure must be small for the two pressures to balance, the pressure within the corner is necessarily close to zero (the saturation pressure). But because the flow is quasisteady, mass lost from the long tapered film is balanced by mass flowing through the corner from the bulk drop. Within the corner, however, p is small; as a result, a pressure–gradient sufficient to drive the mass flow is possible only if the streamwise length of the corner is small: $O(1/\sqrt{\ell_1})$, as shown in figure 3b.

Further simplification is possible. Owing to the small streamwise dimension of the corner, the evaporative mass loss from the film *abcd* proves to be negligibly small. The corner merely acts a funnel, transporting liquid from the bulk drop towards the long tapered film from which it evaporates. Morover, we find (equation 41) that the integrated mass loss from the inner tapered film is determined completely by the outer boundary condition on p. The inner film structure must adjust to satisfy the constraint imposed by mass conservation and the outer boundary condition.

In figure 3b, the square *cdef* indicates the corner for the vapour. Because the Laplace equation contains no length scale, this region is equidimensional. In order that the liquid film affect the vapour merely as a set of boundary conditions on $y = 0$ (as displayed in problem 10), the dimension of this region perpendicular to the substrate must be large compared with the film thickness: $1/\sqrt{\ell_1} \gg h_1\theta_0$. This condition is satisfied provided the contact angle is small, because $\theta \approx h_1\theta_0/(1/\sqrt{\ell_1})$. This ends the discussion of figure 3. We now give the analysis.

5.2. *Inner limit:* $\mathcal{L} \to 0$ *(fixed* h*)*

We shall see that within the region surrounding the apparent contact line, point O in figure 3a, the characteristic film thickness h_1 increases as $\mathcal{L}$ is reduced. Because $h \to 0$ at $-\infty$, to keep h fixed as $\mathcal{L}$ is reduced, we need only move suitably far to the left along the thin tapered film. Within this region, we select a new origin O'. As shown in the figure, we let $\ell_1 = |OO'|$ be the magnitude of the distance between the two origins O and O'. So x' is related to the coordinate x defined in figure 1 by

$$x' = x + \ell_1. \tag{22}$$

We assume that $\ell_1 \to \infty$ as $\mathcal{L} \to 0$; this assumption is verified below (31).

In the following, $\{r', \phi'\}$ denote polar coordinates with respect to O'. In terms of the dimensionless coordinates $\{x, y\}$ defined by (9)

$$r' = \sqrt{(x+\ell_1)^2 + y^2}, \;\; \phi' = \tan^{-1}\left[\frac{y}{x+\ell_1}\right]. \tag{23}$$

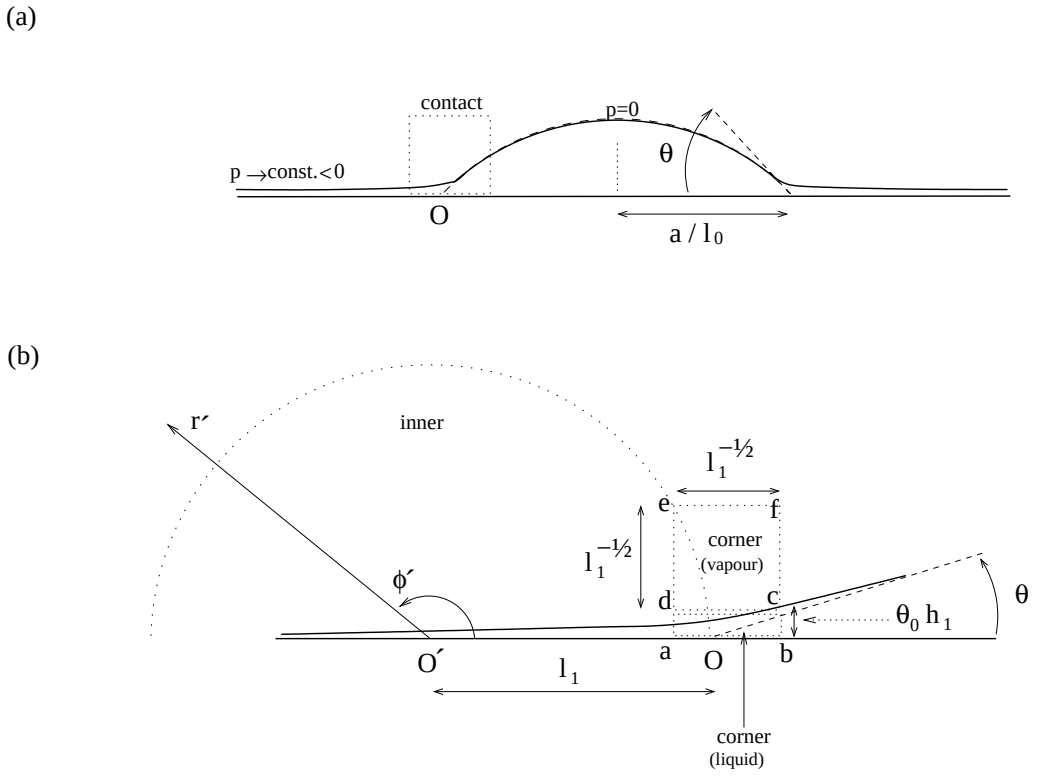

FIGURE 3. Two views of the contact region. (a) Axisymmetric drop having apparent contact line of radius a/ℓ_0. (b) Contact region showing scales for $\mathcal{L} \to 0$: as discussed in the text, $a/\ell_0 \gg \ell_1 \gg 1 \gg 1/\sqrt{\ell_1} \gg h_1\theta_0$. Dimensionless slope unit θ_0, and dimensionless scales h_1 and ℓ_1 are defined by (12) and (31), respectively. Inner and corner regions are defined as the solutions of problems (24) and (39), respectively. All lengths are expressed in the unit ℓ_0.

5.2.1. *Inner problem*

In the limit as $\mathcal{L} \to 0$ (fixed h), problem (10) becomes

$$\nabla^2 p = 0, \text{ for } y > 0. \tag{24a}$$

$$\text{On } y = 0, \; -p = h^{-3}, \tag{24b}$$

$$\frac{\partial}{\partial x'}\Big[h^3 \frac{\partial p}{\partial x'}\Big] + 3\frac{\partial p}{\partial y} = 0. \tag{24c}$$

$$h \to \begin{cases} 0 & \text{as } x' \to -\infty, \\ \infty & \text{as } x' \to \infty. \end{cases} \tag{24d}$$

As $r' \to \infty$,

$$p \sim -\sqrt{r'}\sin\tfrac{1}{2}\phi'. \tag{24e}$$

Problem (24) defines the inner region; by construction, its solution is independent of $\mathcal{L}$.

We note the following properties of (24). First, because the Laplace–Young equation (10b) has been replaced by the algebraic equation (24b), we can not impose the condition

(10f), namely $h \sim bx$. Here, instead, we impose only the weak growth condition (24d); we then determine the asymptotic behaviour of h as $x' \to \infty$ by analysing (24) itself.

Second, as (24e), we have imposed the pressure growth–condition (10e) on the solution of the inner problem. This step is valid because the growth conditions (24d) on h again require that the simplified boundary conditions (3a), (3b) apply, but now far from O' rather than O. The argument leading to (5) still applies, and matching to the outer (Deegan) solution yields (24e). Because the dimensional distance $|OO'|$ is small compared with the drop radius a, negligible error is made by replacing polar coordinates $\{r, \phi\}$ in (5) by $\{r', \phi'\}$.

Third, the maximum evaporative flux from the liquid film is finite, and occurs within this region. Indeed, we have the following asymptotes:

$$-\frac{\partial p}{\partial y}\Big|_{y=0} \sim \begin{cases} 1/(2x'^2) & \text{as } x' \to -\infty \\ 1/(2\sqrt{x'}) & \text{as } x' \to \infty \end{cases} . \qquad (25a, b)$$

As (25a), we repeat (18); to obtain (25b), we need only use (24e) to evaluate the flux. Because the flux vanishes as $x' \to \pm\infty$, it attains a maximum within this region. Let this maximum be f_0. Because f_0 is a property of (24), it is independent of $\mathcal{L}$. This numerical value corresponds to the maximum in evaporative mass described physically by Guéna et al. (2007, p.308).

According to Fick's law, the corresponding maximum dimensional flux is given by

$$-D_v \max_x \frac{\partial \rho_v^*}{\partial y^*}\Big|_{y=0} = f_0 D_v \frac{\Delta\rho_v}{\sqrt{a\ell_0}}. \qquad (26)$$

(Asterisks denote dimensional variables. The ideal gas law, and definitions (9a) and (9c) have been used.) Because (26) is deduced from the inner problem (24), it holds only in the limit as $\mathcal{L} \to 0$.

According to (26), the maximum flux is large compared with that on the surface of the bulk droplet, the latter being of the order of $D_v\Delta\rho_v/a$. The total contribution of the wetting film to mass loss from the drop is, however, smaller than that from the bulk droplet by a factor of the order of $\sqrt{\ell_0/a}$. But, although mass loss from the film is not directly significant in the mass balance for the whole drop, by driving the small–scale flow determining θ, it controls the maximum radius to which the droplet can spread.

We note that, according to (25b), as the bulk drop is approached from within the tapered film, the evaporative mass flux approaches the value given by the Weber solution for the bulk drop. This is occurring even though the tapered film is separated from the bulk drop by the corner region in which the contact angle is formed. Though p_l^* is now sufficiently close to the total gas pressure p_T^* that p_v^* at the interface differs only slightly from the uniform value p_s imposed as a boundary condition on the Weber solution, the difference $p_T^* - p_l^*$ proves sufficiently large to generate the contact angle.

5.2.2. *Scales ℓ_1 and h_1 locating the corner*

To determine the distance $\ell_1 = |OO'|$, we need only find the outer limit of h as $x' \to \infty$. Using (25b) to evaluate the second term in the Reynolds equation (24c), then integrating in x, we obtain

$$\tfrac{1}{3}h^3 \frac{\mathrm{d}p}{\mathrm{d}x'} \sim \sqrt{x'} + c_2. \qquad (27)$$

The integration constant c_2 is determined by mass conservation. Equation (27) represents the inward mass flow per unit within the liquid film. This flow equals the outward flow

per unit time within the vapour; that flow is given by

$$-\int_0^{\pi} \frac{\partial p}{\partial r'}\, r' \mathrm{d}\phi, = \sqrt{r'}. \tag{28}$$

Equation (24e) has been used. Comparing (27) with (28), we see that $c_2 = 0$.

(We note that, according to (28), the total evaporation from the tapered film is determined by mass conservation, and the outer boundary condition (24e). This result is a consequence of the inner–and–outer structure existing in the limit as $\mathcal{L} \to 0$.)

Eliminating p between (24b) and the equation obtained by setting $c_2 = 0$ in (27), then integrating in x', we find that as $x' \to \infty$

$$h \sim c_3 \exp\left[\tfrac{2}{3} {x'}^{3/2}\right]. \tag{29}$$

By the remark following (24), the integration constant c_3 is independent of $\mathcal{L}$.

According to (29), as $x' \to \infty$, the film thickness asymptotically increases exponentially: the disjoining pressure decreases exponentially, whereas the Laplace pressure increases. As a result, the corresponding terms in the Laplace–Young equation balance for sufficiently large h. Using (29) to evaluate $\mathrm{d}^2h/\mathrm{d}x'^2$, we find, without further approximation, that

$$\mathcal{L}h^3 \frac{\mathrm{d}^2 h}{\mathrm{d}x'^2} \sim \mathcal{L}h^4\big(x' + \tfrac{1}{2}x'^{-1/2}\big). \tag{30}$$

According to (30), the capillary and disjoining pressures balance when h and x' satisfy $\mathcal{L}h^4x' \approx 1$; of course, the second term in parentheses in (30) is negligibly small for large x'.

We therefore define scales h_1 and ℓ_1 by

$$\mathcal{L}\ell_1 h_1^4 = 1, \tag{31a}$$

$$\ell_1 = \big(\tfrac{3}{2}\ln h_1\big)^{2/3}. \tag{31b}$$

(Equation (31b) follows by solving (29) for x' in terms of h; we do not include the constant c_3 in the definition of the scales.) The scales $\{h_1, \ell_1\}$ give the dimensionless film thickness and location at which capillary pressure balances disjoining pressure. By determining the distance $\ell_1 = |OO'|$ in figure 3b, equation (31) locates the corner and the characteristic film thickness within it.

The argument leading from (22) to (31) is self–consistent: it is premised on the condition $\ell_1 \gg 1$ and, according to (31), ℓ_1 is logarithmically large in the small parameter $\mathcal{L}$. (Roughly speaking, $h_1 \approx \mathcal{L}^{-1/4}$ and $\ell_1 \approx |\ln \mathcal{L}|^{2/3}$.)

5.2.3. *Dimensions of the corner*

Though (31) locates the corner, it does not determine the increments Δx, Δp and Δh occurring across that region. To determine these, we impose two conditions: within the corner, the capillary pressure is to balance the disjoining pressure; and the mass flow there is to match to that within the inner region. Because, within the inner region, the mass flow is given by $-h^3 \frac{\mathrm{d}}{\mathrm{d}x} h^{-3}, = \frac{\mathrm{d}}{\mathrm{d}x} \ln h$, we have the following:

$$\frac{1}{h_1^3} = \Delta p = \mathcal{L}\frac{\Delta h}{\Delta x^2}; \tag{32a,b}$$

$$h_1^3 \frac{\Delta p}{\Delta x} = \sqrt{\ell_1}. \tag{32c}$$

We have used (27) to evaluate the mass flow at the outer edge of the inner region.

Solving (32), we obtain

$$\Delta x = 1/\sqrt{\ell_1}, \;\; \Delta h = 1/\sqrt[4]{\mathcal{L}\ell_1}, \tag{33a,b}$$

$$\Delta p = (\mathcal{L}\ell_1)^{3/4}. \tag{33c}$$

In the form $h_1 = 1/\sqrt[4]{\mathcal{L}\ell_1}$, equation (31a) has been used. We note that because these scales are obtained from the Laplace–Young condition and the film mass balance, they describe the liquid film within the region shown as *abcd* in figure 3b.

According to (33a), the x–dimension of the corner is vanishingly small compared with the length ℓ_1 of the tapered film. This is so because the total mass evaporated from the long tapered film is $O(\sqrt{\ell_1})$, by (32c). Because the film thickness and streamwise pressure difference Δp across the corner satisfy $h_1^3 \Delta p = 1$, mass conservation requires the streamwise length of the corner to be $O(1/\sqrt{\ell_1})$. This is the basis of the physical explanation given in the discussion of figure 3b.

Variables (with circumflexes) for the corner are defined accordingly:

$$\{x, y\} = \{\hat{x}, \hat{y}\}/\sqrt{\ell_1}, \;\; h = \hat{h}/\sqrt[4]{\mathcal{L}\ell_1}, \tag{34a,b}$$

$$p = (\mathcal{L}\ell_1)^{3/4}\hat{p}. \tag{34c}$$

In (34a), we are using the origin O at the apparent contact line; the translated origin O' has been used only to describe the inner region.

For use below, we give the relations between the corner variables (34) and dimensional quantities:

$$\{x_*, y_*\} = \frac{(ad^2)^{1/3}}{k^{2/3}\ell_1^{1/2}}\,\{\hat{x}, \hat{y}\}, \tag{35a}$$

$$h_* = \frac{(ad^2)^{1/6}}{k^{1/3}\ell_1^{1/4}}\Big(\frac{A}{\gamma}\Big)^{1/4}\hat{h}. \tag{35b}$$

The pressure difference across the interface is given by

$$p_l^* - p_T = k\frac{\nu_l D_v \Delta\rho_v}{a^{1/2}}\Big(\frac{\gamma}{A}\Big)^{3/4}\ell_1^{3/4}\,\hat{p}. \tag{35c}$$

5.2.4. *Existence of a separation of pressure scales*

Before using the corner variables to manipulate the governing equations, we discuss the physical significance of the pressure equation (34c). First, because the pressure boundary condition (24e) underlies the entire structure of the corner, we verify that the magnitude of the pressure within the corner is consistent with the boundary condition used to obtain (24e): namely $\lim_{r'\to\infty} p = 0$.

To do so, we compare the pressure scale $\Delta p = (\mathcal{L}\ell_1)^{3/4}$ in (34c) with the maximum pressure $p_{\max}$ within the vapour at the same distance ℓ_1 from the origin O'. According to (24e), for fixed r, the maximum pressure within the vapour occurs along the tapered film at $\phi' = \pi$. Consequently, at $r' = \ell_1$, $p_{\max} \approx \ell_1^{1/2}$, and $\Delta p/p_{\max} \approx (\ell_1\mathcal{L}^3)^{1/4}$. Because ℓ_1 is only logarithmically large in the small parameter $\mathcal{L}$, we see that

$$\lim_{\mathcal{L}\to 0} \Delta p/p_{\max} = 0 : \tag{36}$$

within the corner, the pressure in the vapour is vanishingly small compared with the maximum pressure in the vapour at that radius ℓ_1. Equation (34c) is therefore consistent with the boundary condition on which (24e) is based.

Second, although the pressure in the corner *abcd* is *small* compared with the maximum

pressure within the vapour, it is *large* compared with the estimate that we would obtain for p by evaluating the outer boundary condition (24e) at the liquid–vapour interface. This important condition ensures that, in the corner, the flow within the liquid film does not see a pressure–gradient imposed by the flow outside the film. Instead, the pressure within the film adjusts to supply the mass being evaporated within the inner (tapered film) region.

To prove this condition, we first note that, within the corner, the film thickness is $\approx h_1\theta_0$, as shown in figure 3b. From figure 3b, we estimate that, within the corner at the liquid–vapour interface, $\phi' \approx h_1\theta_0/\ell_1$, where $\theta_0 = h_0/\ell_0$ is given by (12b) and h_1 by (31a).

Using this estimate for ϕ' to evaluate the outer boundary condition (24e) at the liquid–vapour interface, and denoting by $p_{\text{est.}}$ the pressure estimate so obtained, we have

$$p_{\text{est.}} \approx \theta_0 \frac{h_1}{\ell_1^{1/2}}, \approx (\mathcal{L}/\ell_1)^{3/4} \frac{A}{\gamma L^2}. \tag{37}$$

Equation (31a) has been used to eliminate h_1; also (11) has been used in the form $\theta_0 = A\mathcal{L}/(\gamma L^2)$;

Comparing (37) with the corner scale (33c), we see that $p_{\text{est.}}/\Delta p \approx \ell_1^{-3/2}$. Because ℓ_1 is logarithmically large in the small parameter, it follows that

$$\lim_{\mathcal{L}\to 0} p_{\text{est.}}/\Delta p = 0, \tag{38}$$

the limit being taken with $\gamma L^2/A$ fixed. As claimed, the pressure estimated from (24e) is vanishingly small compared with the pressure scale (33c) set by the mass balance within the liquid film. Were this not so, the film flow within the corner would interact with the vapour flow outside and, to represent that interaction, we would need to include in (34c) an additional additive pressure scale.

Equations (36) and (38) can be summarized by stating that for $\mathcal{L} \to 0$, there is separation of pressure scales: $p_{\text{est.}} \ll \Delta p \ll p_{\max}$. Because the pressure within the film (and adjacent vapour) is small compared with the maximum pressure at the radial location of corner, it does not modify the external pressure field whose asymptotic form for large r' is given by (24e). At the same time, when evaluated at the liquid–vapour interface, the external pressure (24e) is small compared with the pressure in the film; as a result, it does not perturb the liquid flow. We will now see the implication of this separation of scales.

5.3. *Vapour flow in the corner*

5.3.1. *Governing equations and self–consistency*

Expressing (10a) to (10c) in terms of the corner variables, without approximation, we find that within the rectangular domain *cdef* in figure 3b, the vapour pressure $\hat{p}$ satisfies

$$\hat{\nabla}^2 \hat{p} = 0. \tag{39a}$$

On $\hat{y} = 0$

$$-\hat{p} = \frac{\mathrm{d}^2\hat{h}}{\mathrm{d}\hat{x}^2} + \hat{h}^{-3}, \tag{39b}$$

$$\frac{\partial}{\partial \hat{x}}\left[\hat{h}^3 \frac{\partial \hat{p}}{\partial \hat{x}}\right] + 3(\ell_1 \mathcal{L}^3)^{1/4} \frac{\partial \hat{p}}{\partial \hat{y}} = 0. \tag{39c}$$

(Because growth conditions (10e) and (10f) are unchanged, they are not repeated here.) Together (39b) and (39c) provide the boundary condition for $\hat{p}$ along the base *cd* of the

rectangular domain shown in figure 2b; conditions on the other three sides of the domain would be provided as matching conditions on $\hat{p}$.

We need not enter into that detail, however. Because ℓ_1 is only logarithmically large in the small parameter $\mathcal{L}$, the coefficient of $\partial\hat{p}/\partial\hat{y}$ in (39c) vanishes as $\mathcal{L} \to 0$. Consequently, the mass flux along the film is independent of position within the corner. This is reasonable because the corner is small, and the mass transport varies only slowly in x at the outer edge of the inner region. Because the simplified boundary conditions (39b) and (39c) no longer contain derivatives normal to the boundary, they form a pair of simultaneous equations determining $\hat{p}(x,0)$ and $\hat{h}$. Within the rectangular region *cdef* shiwn in figure 3b, the diffusion field therefore responds passively to the perturbation pressure imposed along side *cd* by the liquid film. Because we are concerned with contact angle, we need not discuss boundary conditions for (39a) on the other three sides of the domain.

Integrating the simplified form of (39c), we obtain

$$\hat{h}^3 \frac{\partial \hat{p}}{\partial \hat{x}} = c_4. \tag{40}$$

The constant c_4 is determined by matching the mass flow.

At the outer edge of the inner tapered film, the mass flow is given by (27):

$$\tfrac{1}{3} h^3 \frac{\partial p}{\partial x'} = \sqrt{x'}. \tag{27$'$}$$

Without approximation, we use (22) and the definitions (34) to express (27) in terms of corner variables:

$$\tfrac{1}{3} \hat{h}^3 \frac{\partial \hat{p}}{\partial \hat{x}} = \left(1 + \hat{x}/\ell_1^{3/2}\right)^{1/2}.$$

Taking the limit as $\ell_1 \to \infty$ ($\hat{x}$ fixed, possibly large), we find that

$$\hat{h}^3 \frac{\partial \hat{p}}{\partial \hat{x}} = 3, \tag{41}$$

at the outer edge of the inner region. With equation (41), we establish the claim made in §5.1: the total evaporation–rate from the inner tapered film is determined completely by mass conservation, and the outer boundary condition (24e). Further, comparing (41) with (40), we see that the mass flow is matched provided $c_4 = 3$.

Using the separation of pressure scales existing for small $\mathcal{L}$, we have shown that determining the contact angle does not require solving the Laplace equation for the corner. Instead the problem reduces to that of solving an ordinary differential equation. Without this simplifying property of the limit as $\mathcal{L} \to 0$, the liquid and vapour flows are fully coupled throughout the domain illustrated in figure 2, and the Laplace equation must be solved simultaneously with the other members of (39).

5.3.2. *Boundary–value problem for $\hat{h}$.*

Substituting (39b) into (40), we find that for $-\infty < \hat{x} < \infty$

$$\tfrac{1}{3} \hat{h}^4 \frac{\mathrm{d}^3 \hat{h}}{\mathrm{d}\hat{x}^3} = \frac{\mathrm{d}\hat{h}}{\mathrm{d}\hat{x}} - \hat{h} \tag{42a}$$

$$\text{As } \hat{x} \to -\infty, \ \frac{\mathrm{d}\hat{h}}{\mathrm{d}\hat{x}} - \hat{h} \to 0. \tag{42b}$$

$$\text{As } \hat{x} \to \infty, \ \frac{\mathrm{d}^2 \hat{h}}{\mathrm{d}\hat{x}^2} \to 0. \tag{42c}$$

Equation (42b) expresses the condition that, within the liquid film, the pressures are matched within the overlap region connecting the corner to the inner region. To prove this, we first express (22) in the form $x' = \ell_1 + \hat{x}/\ell_1^{1/2}$. Substituting this expression, without approximation, into (29), we find that at the outer edge of the inner tapered film, the film thickness is given by

$$h \sim c_3 \exp\left[\tfrac{2}{3}\ell_1^{3/2}\big(1+\hat{x}/\ell_1^{3/2}\big)^{3/2}\right]. \tag{43}$$

Using (34b) to express (43) in terms of the corner variable $\hat{h}$ and noting that (31) can be written as $(\mathcal{L}\ell_1)^{1/4}\exp(\frac{2}{3}\ell_1^{3/2}) = 1$, we obtain

$$\hat{h} \sim c_3 \exp\left[\tfrac{2}{3}\ell_1^{3/2}\big[\big(1+\hat{x}/\ell_1^{3/2}\big)^{3/2}-1\big]\right],$$

without approximation. It follows that in the limit as $\ell_1 \to \infty$ (fixed $\hat{x}$)

$$\hat{h} \sim c_3 \mathrm{e}^{\hat{x}}. \tag{44}$$

This is equivalent to (42b).

Because problem (42) is invariant under translation in $\hat{x}$, boundary condition (42b) is sufficient to ensure that the corner film thickness could be matched to (44) for the value of c_3 imposed by the solution of the inner problem (24). Because the film thickness can be matched, and $p \sim -h^{-3}$ within the overlap region, so too can the pressure.

Problem (42) can be expressed as equivalent problem determining film slope $\mathrm{d}\hat{h}/\mathrm{d}\hat{x}$ as a function of film thickness $\hat{h}$; for this reason, we do not need the constant c_3 entering into (44). Appendix A describes the method used to compute the solution of (42).

6. Predicted contact angle

Figure 4 shows $\mathrm{d}\hat{h}/\mathrm{d}\hat{x}$ computed as a function of film thickness $\hat{h}$ from (42). According to equation (A.6)

$$\lim_{\hat{h}\to\infty} \frac{\mathrm{d}\hat{h}}{\mathrm{d}\hat{x}} = c_6, = 1.47758\ldots. \tag{45}$$

At $\hat{h} = 10$, $\mathrm{d}\hat{h}/\mathrm{d}\hat{x}$ is within about 4% of the limiting value (45); at that point, $\hat{p} = -0.1045\ldots$.

The contact angle here differs in one essential from that occurring during isothermal spreading. According to (45), at the outer edge of the contact region of the stationary evaporating meniscus, the slope approaches a limit. This is also true for the stationary meniscus when evaporation is limited by heat conduction through the liquid (Morris 2001). In both cases, the slope approaches a limit because the volume flow rate along the liquid film is independent of position at the outer edge of the contact region, causing $\mathrm{d}^3h/\mathrm{d}x^3$ to vary asymptotically as h^{-3}. As a result, h is asymptotically a linear function of x. For these two problems in which the apparent contact line is stationary, the contact angle is independent of the large–scale geometry of the interface; this is so, *provided* the pressure difference across the interface at the outer edge of the corner region is small compared with the pressure difference (35c) within the corner. If this condition is satisfied, problem (10) completely determines θ, and the outer geometry affects θ only through the outer boundary condition (10d).

The behaviour is different when the contact line moves relative to the substrate. Relative to axes moving with the contact line, the volume flow rate then increases linearly with film thickness, causing $\mathrm{d}^3h/\mathrm{d}x^3$ to vary asymptotically as h^{-2} (Morris 2001, p.28).

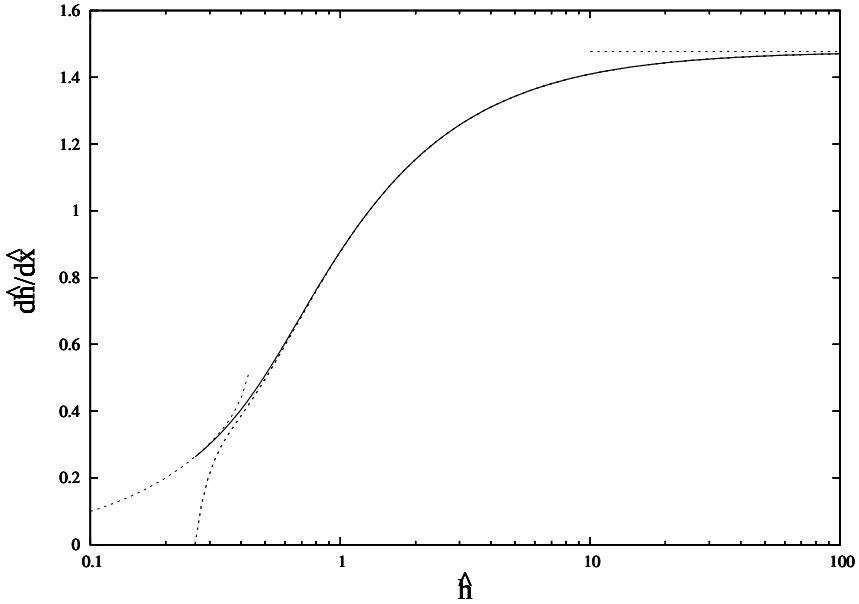

FIGURE 4. Solid curve, numerical solution of (42); broken curves, asymptotes: (A.3), $\hat{h} \to \infty$ and (A.5), $\hat{h} \to 0$; broken line, limiting value (45).

As a result, the film thickness grows more rapidly than x, and the contact angle is *always* influenced by the geometry of the large–scale interface. For the problem of isothermal spreading, this is discussed in the review article of Bonn et al. (2009, p.766).

For $\mathcal{L} \to 0$, the contact angle is given in terms of the dimensional quantities h_* and x_* by

$$\lim_{\hat{h}\to\infty} \frac{\mathrm{d}h_*}{\mathrm{d}x_*} \sim c_6 k^{1/3} \frac{A^{1/4}}{\gamma^{1/4} a^{1/6} d^{1/3}} \ell_1^{1/4}. \tag{46}$$

Equations (35a) and (35b) have been used. As stated in §1, in this work, the swung dash is used only to indicate an asymptotic relation.

Equation (46) holds if mass transfer occurs by pure diffusion at the drop scale. As noted below (5), when buoyant convection is significant at that scale, the factor k becomes a function of the parameters controlling that convection. According to table 1, the value of $\mathcal{L}$ is also affected by k, through the slope unit θ_0; that effect is secondary because in (46) only ℓ_1 depends on $\mathcal{L}$ and, as stated below (31), that dependence is weak.

Substituting for d from (8) and using $c_6 k^{1/3} = 1.427$, we obtain

$$\theta \sim 1.427\, \mathcal{D}^{1/3} \sqrt[4]{\ell_1}; \tag{47}$$

as given in table 1,

$$\mathcal{D} = \frac{\nu_l D_v \, \Delta\rho_v}{(A\gamma^3 a^2)^{1/4}}. \tag{48}$$

With equation (47), we have overcome the difficulty described at the end of §3. Though, in general, θ depends on two parameters, $\mathcal{L}$ and θ_0, each depending significantly on A, we have shown that for small $\mathcal{L}$, these parameters combine to form the density parameter $\mathcal{D}$. Whereas the general relation (12) permits θ to depend on A in an arbitrary fashion, this dependence is weak in the experimentally interesting case: according to (47), $\theta \propto A^{-1/12}$.

519 This is significant because the value of A is affected by contamination of the surface, as
520 discussed e.g. by Truong and Wayner (1987) and Israelachvili (1991, p.196).

521 Although θ depends to a first approximation only on the parameter $\mathcal{D}$, it continues to
522 depend weakly on $\mathcal{L}$ through the factor $\sqrt[4]{\ell_1}$ in (47). As discussed in the context of figure
523 5, below, this dependence on $\mathcal{L}$ can be noticeable under some conditions.

524 7. Interpretation using scaling

525 The formula for θ corresponds to a definite picture of the contact region. As the
526 Laplace parameter is reduced, at a fixed value of film thickness, the disjoining pressure
527 dominates the capillary pressure. Because the capillary pressure is essential to contact
528 angle formation, that process can occur, for small $\mathcal{L}$, only once the film has become
529 relatively thick. As a result, there is a long section of precursor film from which liquid
530 can evaporate; in comparison with the evaporation from the precursor film, that from
531 the region generating the contact angle is negligibly small.

532 To consolidate this picture, we combine it with scaling to obtain the form of (47). Let p_l,
533 h and ℓ be the dimensional liquid pressure, and characteristic dimensions of the corner
534 region within which the angle is formed. This region has two defining characteristics.
535 First, the capillary pressure balances the disjoining pressure: $p_l \approx \gamma h/\ell^2 \approx A/h^3$, the
536 latter equation requiring h to be the geometric mean of ℓ and $(A/\gamma)^{1/2}$. Second, within
537 the liquid film, the mass flow rate J per unit length of contact line is independent of
538 position: $h^3 p_l/(\nu_l \ell) \approx J$. These three equations determine the unknowns $\{p_l, h, \ell\}$ in
539 terms of the constant J.

Solving for h and ℓ, we obtain

$$h \approx \frac{A^{3/4}}{\gamma^{1/4}(\nu_l J)^{1/2}}, \quad \ell \approx \frac{A}{\nu_l J}. \tag{49a,b}$$

According to equation (27) of the small–$\mathcal{L}$ analysis, J scales with the fundamental units h_0 and ℓ_0, but is increased by a factor $\ell_1^{1/2}$ reflecting the length of the tapered film:

$$J \approx \frac{h_0^3}{\nu_l \ell_0}\left(\frac{\rho_l}{\rho_s}\sqrt{\frac{\ell_0}{a}}\Delta p_v\right)\ell_1^{1/2}.$$

(The term in parentheses is the scale for liquid pressure, as given by (9c).) Substituting for h_0 and ℓ_0 from (7), we find that

$$\frac{J}{D_v \Delta\rho_v} \approx \left(\frac{d}{a}\right)^{1/3}\ell_1^{1/2}; \tag{50}$$

540 $d = A/(\nu_l D_v \Delta\rho_v)$, as defined by (8).

541 To interpret (50), we recall that the rate of mass loss from the bulk droplet is $\frac{2}{\pi} D_v \Delta\rho_v$,
542 per unit of contact line (Cazabat and Guéna 2010, equation 7). According to (50), the
543 additional rate of mass loss across the wetting film is small compared with that from the
544 bulk drop provided $a \gg d$, that is, provided the notion of an apparent contact line is
545 applicable.

Eliminating $\nu_l J$ between (49) and (50), we obtain

$$h \approx (a^2 d)^{1/3}\left(\frac{A}{\gamma a^2}\right)^{1/4}\ell_1^{-1/4}, \quad \ell \approx (a d^2)^{1/3}\ell_1^{-1/2}. \tag{51a,b}$$

546 To within a numerical factor, these results are equivalent to those given by (35).

547 The scaling relation $\theta \approx \mathcal{D}^{1/3}$ corresponding to (47) follows on using $\theta \approx h/\ell$. Poulard

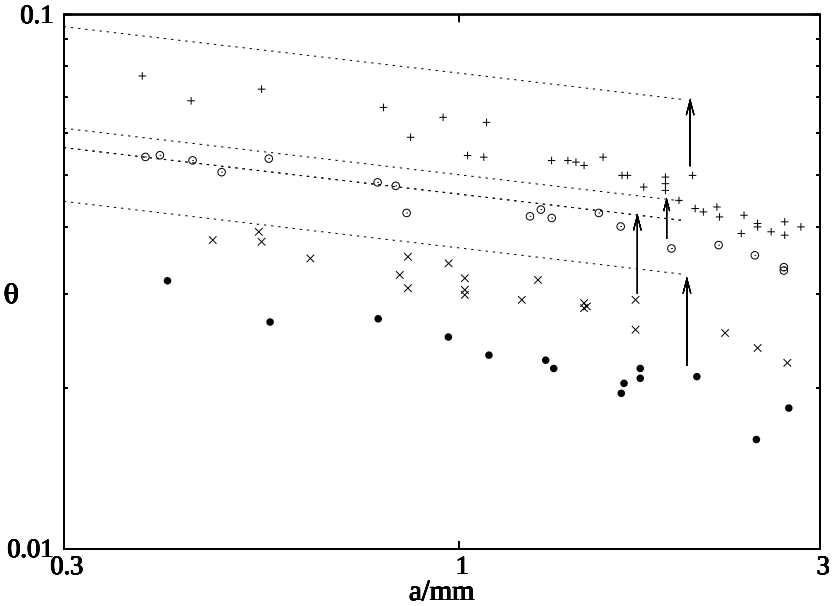

FIGURE 5. Measured and predicted angles. Symbols, Guéna data: in order of increasing $\mathcal{L}$, • nonane $0.00046 < \mathcal{L} < 0.00075$; × OMTS $0.0014 < \mathcal{L} < 0.0026$; ∘ octane $0.0025 < \mathcal{L} < 0.0045$; + HMDS $0.022 < \mathcal{L} < 0.041$. Arrows guide the eye from the data to the line showing the angle predicted by (47) for that fluid. Lines end at $a = 2$ mm. There are no adjustable parameters.

et al. (2005) also use scaling to obtain a cube root relation, but their physical picture differs from ours: theirs contains a triple junction near which the Laplace pressure balances the disjoining pressure, and the neighbourhood of that triple junction is assumed to influence the observed contact angle.

8. Comparison with experiment

8.1. *Contact angles*

Figure 5 shows the measured and the predicted values. Only values for drops having $0.3 < a/\text{mm} < 3$ are shown; this range was chosen to cover a decade in the logarithmic scale, and to include all experimental data showing the $a^{-1/6}$ scaling identified by Guéna et al (2007, p.312). As broken lines, we show the prediction (47); because $\ell_1^{1/4}$ varies slightly along each line, the arithmetic mean of the maximum and minimum values was used to obtain the coefficient in (47); using this approach, the predicted values of $\theta/\mathcal{D}^{1/3}$ are 1.60 (octane), 1.62 (OMTS), 1.67 (nonane) and 1.49 (HMDS).

There are no adjustable parameters in this comparison. Appendix B gives the values of material properties used in making the figure. Of these, only the value of A is uncertain and, according to (47), θ is insensitive to A. Values for the diffusion coefficient D_v used here are, in all cases, about twice those given by Cazabat & Guéna (2010, table 2); there is further detail in the appendix.

The figure caption gives the range of $\mathcal{L}$–values for each fluid. Owing to the differing material properties, for a given value of a, $\mathcal{L}$ decreases from the top of the figure to the bottom. For a given fluid, $\mathcal{L}$ decreases from left to right because $\mathcal{L} \propto a^{-2/9}$, as shown by table 1.

Fair agreement is obtained between measured and predicted angles: for $a = 1$ mm, the ratio of the observed to predicted values is about 0.9 (octane), 0.8 for HMDS and 0.7 for

nonane and OMTS. Two properties of the figure suggest that a mechanism not included in (10) is needed to explain the detailed behaviour, however. First, for each fluid, the data approach the appropriate small–$\mathcal{L}$ asymptote towards the left of the figure, where the value of $\mathcal{L}$ for the fluid is largest (but still less than unity). Though the approach occurs in the opposite sense to that expected of an asymptote depending on a single parameter, this behaviour is consistent with the suggestion by Cazabat & Guéna (2010, §VI.4) that a second scale of motion is needed to explain the behaviour of larger drops.

Second, the trend from one fluid to another is not monotonic. The gap between the asymptote and data decreases from HMDS to octane; this is consistent with $\mathcal{L}$ being an order of magnitude smaller for octane. For the next fluid OMTS, however, the values of $\mathcal{L}$ are slightly less than of octane, but the gap is much larger. The gap is also large for nonane, even though the values of $\mathcal{L}$ for it are about one–third those for OMTS. Because octane and OMTS have almost the same values of $\mathcal{L}$, the non–monotonicity can not be a consequence of the approximate nature of (47); some effect not included in (10) is required.

8.2. *Film thickness at which θ forms*

By (45), at $\hat{h} = 10$ the slope is within 4% of its limiting value: the corresponding dimensional film thickness is

$$h_\theta = 10k'(ad^2)^{1/6}\left(\frac{A}{\gamma}\right)^{1/4}. \tag{52}$$

Equation (35b) has been used. The dimensionless factor $k' = k^{-1/3}\ell_1^{-1/4}$; assuming mass transfer at the drop scale to be by pure diffusion, $k' \doteqdot 1$ to within about 15% for values of $\mathcal{L}$ occurring in the experiments.

In table 2 we give predicted values of h_θ for two cases for which experimental values can be estimated, at least roughly. Line 1 gives the scales for a 1 mm octane droplet. For this case, the uppermost curve in figure 5a of Guéna et al.(2007) gives the corresponding film profile measured at reversal; the contact angle appears to be well–defined at the second fringe, the corresponding film thickness being of the order of 200–300 nm. Though this is about four times the predicted value, more precise agreement is not to be expected because for this case there are too few interference fringes to resolve the contact region.

As we would expect from figure 5, the discrepancy between predicted and observed values of h_θ increases with drop size. Line 2 gives the scales for 9 mm droplet of OMTS. According to figure 5b of Guéna et al. (2007a), for droplets of OMTS having $1 < a/\mathrm{mm} < 9$, the angle is observed to form at a thickness $h_\theta \approx$ 1–2 μm; the scale increases weakly with a. Though the trend is consistent with (52), the observed value is 10–20 times that predicted.

Let us review possible causes of this discrepancy. We have assumed that mass transfer at the droplet scale is by pure diffusion. Though, as noted in §1, for 8 mm drop of heptane (a fluid with properties comparable with those of OMTS), the Nusselt number $Nu \approx 3$, this does not seem large enough to explain an order of magnitude discrepancy in h_θ, particularly because that scale is relatively insensitive to k, varying only as its one–third power. (Here, we are of course assuming that the basis function in (5a) is unchanged even as Nu increases above unity.)

Second, our quantitative predictions from (10) are based on the assumption of a separation of scales ($\ell_1 \gg 1$) holding in the limit as $\mathcal{L} \to 0$. According to table 2, however, for the experimental conditions $\ell_1 \approx 2$. This, however, is also unlikely to explain the discrepancy. There is no reason for the assumption $\ell_1 \gg 1$ to be adequate for small

drops, but to fail for the large ones: because $\mathcal{L}$ varies as $a^{-2/9}$, the approximation should improve with increasing drop size.

Third, the equation $\Pi = Ah^{-3}$ for disjoining pressures holds only over a very short range of film thicknesses, as discussed below (1). It should, however, be a good approximation within the thin tapered film in which, according to the discussion in §5.2.1, evaporation from the contact region is concentrated. Though for $h < 1$ nm, the h^{-3} relation begins to fail because the continuum film begins to resemble an adsorbed layer, we know from §5 that, in the limit as $\mathcal{L} \to 0$, the inner tapered film affects θ only through the total rate of evaporation within it. This quantity is, however, itself determined by the outer boundary condition, as shown by (41). Because the structure of the tapered film adjusts to the constraint imposed by mass conservation and the outer boundary condition, failure of the h^{-3} relation for small film thicknesses seems unlikely to explain the discrepancy between predicted values of θ, and those observed for large drops.

At the other extreme, when h is sufficiently large, retardation becomes significant, and the disjoining pressure approaches the asymptote $\Pi \propto h^{-4}$; see Truong and Wayner (1987, figure 6), Israelachvili (1992, §11.7). Though this form is likely to be appropropriate within the corner, its effect will be to make problem (42) more nonlinear. This should weaken the dependence of θ on a, rather than producing the stronger dependence observed for $a > 1$ mm. (This heuristic argument is readily verified by scaling. Using the h^{-4} relation in the steps leading to (49), but retaining the h^{-3} relation in (50), we find that $\theta \propto a^{-1/7}$; this is weaker than the dependence given by the original argument.) Using another form for disjoining pressure Π seems unlikely to improve the ability of theory to predict the behaviour of larger drops.

Cazabat and Guéna (2010, §VI.4) propose that larger drops depart from the relation $\theta \propto a^{-1/6}$ because the capillary number of the liquid flow at the scale a becomes larger than unity; as result, 'hydrodynamic flow and drop shape are no longer independent, and a second intermediate characteristic length scale is clearly required.' Scaling of (14) verifies that if the Bond number $\rho_l g a^2/\gamma \gg 1$, gravitational flattening of the drop does increase the pressure gradient needed to drive flow towards the contact line.

Because the slope calculated from the local formulation (10) approaches a limit at the outer edge of the contact region, we know the two defining properties of the second scale (ℓ_2, say) proposed by Cazabat and Guéna. First, for the largest drops ($a = 9$ mm) studied by Guéna (2007), the measured angle is about one–half that predicted by (47); the product of ℓ_2 with the interface curvature characterizing the second region is, therefore, of the order of θ. Second, this curvature is determined by the pressure–difference needed to drive the large–scale flow from the centre of flattened drop towards the contact region. These conditions characterize the proposed second region.

Further, because the first interference fringe occurs at a film thickness of the order of 0.1 μm, comparable with the thickness at which the present analysis predicts θ to form, we speculate that two separate contact angles might exist at scales whose separation increases with drop size. For the advancing heated meniscus, a similar possibility is proposed by Morris (2001, p.28). Detailed analysis of the drop–scale flow is beyond the scope of this work, however.

9. Conclusion

Motivated by the experiments of Guéna et al. (2007a), we have posed the boundary–value problem (10) governing the contact region of an evaporating drop at the instant it reaches its maximum radius a. In §4, we have shown that the formulation is self–consistent. In particular, the notion of an apparent contact line having a well–defined

	d (nm)	L (nm)	a (mm)	h_0 (nm)	ℓ_0 (nm)	$\mathcal{L}$	h_1	ℓ_1	h_θ (nm)
octane	3.1	0.15	1	1.7	230	0.00382	3.6	1.5	60
OMTS	5.3	0.15	9	2.5	680	0.00137	4.5	1.7	110

TABLE 2. Scales for two droplets: h_θ is defined by (52).

radius is applicable if there is a separation of length scales:

$$a \gg d; \tag{53}$$

the macroscopic scale a must be large compared with the disjoining–diffusion length $d = A/(\nu_l D_v \Delta\rho_v)$, as defined by (8). We have shown that when (53) holds, there is also a separation of time scales: the contact region then evolves on a time scale short compared with that on which the bulk drop evolves (at the instant of reversal). As a result, there is no time–derivative in (10).

The solution of (10) depends on one parameter $\mathcal{L}$, a dimensionless surface tension. Though the formulation is valid for arbitrary values of $\mathcal{L}$, we have analysed the special case $\mathcal{L} \to 0$ corresponding to small surface tension. In the experiments $\mathcal{L}$ ranges from 0.0005 to 0.04; for a given fluid, $\mathcal{L}$ decreases with increasing drop size.

In the limit as $\mathcal{L} \to 0$, there is a further separation of length scales within the contact region itself. Evaporation from this region is now confined to a long thin tapered wetting film extending radially outwards from the drop; the dimensionless streamwise length ℓ_1 of this film is asymptotically large in the small parameter $\mathcal{L}$. Within the film, the capillary pressure is negligibly small. As the bulk drop is approached, the film thickens and, as a result, the disjoining pressure decreases, allowing it to be balanced by the capillary pressure within a corner region whose streamwise dimension vanishes as $\ell_1^{-1/2}$. The contact angle is formed within this small region.

This structure has implications for the distribution of evaporative mass flux. At the inner edge of the corner, facing the drop centre, the liquid pressure rises towards the total pressure in the gas. As a result, the vapour pressure p_v on the interface falls to the (constant) saturation value p_s, and the evaporative mass flux across the interface matches to that given by the Weber disc solution. Within the corner, and wetting film, the liquid pressure p_l is sufficently low that the vapour partial pressure at the interface is coupled to the liquid flow through the Gibbs–Thomson relation. This brings us to the key simplifying feature of the small–$\mathcal{L}$ analysis.

In the limit as $\mathcal{L} \to 0$, evaporation from the corner proves to be negligibly small. As a result, the corner acts as a funnel feeding liquid from the drop to the long thin evaporating film. This has two implications. Within the corner, film thickness is determined completely by the liquid flow; consequently, the film profile is determined by an ordinary differential equation, rather than by a coupled system involving the steady diffusion equation for the vapour.

Further, because evaporation is negligibly small within the corner, and the Gibbs–Thomson (Kelvin) effect is negligibly small within the bulk drop, *for the purpose of calculating the evaporative mass flux* the difference between p_v^* and p_s is significant only within the thin tapered film. To evaluate it there, the pressure difference $p_T - p_l$ across the interface can be replaced by the disjoining pressure; see (24b).

This result illuminates an approximation made by Eggers and Pismen (2010) in their simulation of an evaporating sessile drop. In their equation (25) for the evaporative mass

flux, it is assumed that the pressure jump across the interface can be approximated by the disjoining pressure 'since van der Waals forces dominate in the contact line region'. According to the discussion above, this approximation amounts to assuming, at least implicitly, a separation of scales.

We have made a careful comparison between predicted and measured angles. According to the experiments of Guéna et al. (2007a), the contact angle θ measured at the inflexion point varies as $a^{-1/6}$ for $a < 1$ mm (about); for larger drops, $\theta \propto a^{-n}$, the exponent n then being fluid–specific. For drops obeying the $a^{-1/6}$ rule, predicted and measured angles agree to within 10–30%; the discrepancy increases with drop size, and is fluid–specific. Because $\mathcal{L}$ varies inversely with drop size for a given fluid, we infer that some effect not included in (10) is required to explain the behaviour of larger drops. In particular, we note that measured and predicted angles may refer to quantities occurring at scales which coincide for small drops, but become increasingly separated with increasing drop size. Numerical solutions, of (10) and of the initial–value problem for the whole drop, will be made to investigate this possibility.

I am grateful to Professor C.J. Radke and to the reviewers for comments that helped me improve the presentation and, above all, to Professor A.–M. Cazabat for helpful discussions about the experiments.

Appendix A. Solution of (42)

We introduce dummy variables x and y defined by

$$\hat{x} = x, \;\; \hat{h} = 3^{1/4} y. \tag{A.1}$$

Because these variables are used only in this appendix, they can not be confused with the coordinates $\{x, y\}$ used in the text.

Substituting (A.1) into (42), then introducing y as the independent variable, we find that $z = \mathrm{d}y/\mathrm{d}x$ satisfies the following problem. For $0 < y < \infty$

$$y^4 z \frac{\mathrm{d}}{\mathrm{d}y}\left[z \frac{\mathrm{d}z}{\mathrm{d}y}\right] = z - y. \tag{A.2a}$$

$$\text{As } y \to \infty, \; z \to c. \tag{A.2b}$$

$$\text{As } y \to 0, \; z \sim y. \tag{A.2c}$$

The constant c is found as part of the solution.

To find the form of the solution, we let $z = c + \zeta$. Because (A.2b) requires that $\zeta \ll c$ for $y \to \infty$, the left side of (A.2a) can be linearized, and the right hand side approximated by $-y$. With these simplifications, we find that $y^3 c^2 \mathrm{d}^2\zeta/\mathrm{d}y^2 \sim -1$. So $\zeta \sim c_0' y + c_1' - 1/(2c^2 y)$, where (A.2b) requires that the constants $c_0' = 0 = c_1'$. We conclude that for $y \to \infty$, the solution of (A.2) depends on the single parameter c, and that $z \sim c - 1/(2c^2 y)$. (We may also reach this conclusion by linearizing the left side of (A.2a) as above, but without approximating the right hand side. This leads to the modified Bessel equation; the conclusion then follows from known properties of its solutions.)

So, for $y \to \infty$, the solution of (A.2) has the asymptote

$$z \sim c + \sum_{n=1}^{\infty} a_n y^{-n}. \tag{A.3}$$

Substituting (A.3) into (A.2a), then equating coefficients of y^{-n}, we obtain

$$a_1 = -\frac{1}{2c^2},\ \ a_2 = \frac{4c^4-5}{24c^5},\ \ a_3 = \frac{28c^4-41}{288c^8}, \qquad (A.4a,b,c)$$

$$a_4 = -\frac{20c^8-139c^4+168}{1440c^{11}}, \qquad (A.4c,d)$$

$$a_5 = -\frac{4240c^8-18176c^4+18207}{172800c^{14}}, \qquad (A.4e)$$

$$a_6 = \frac{67200c^{12}-1122160c^8+3457088c^4-2936031}{29030400c^{17}}. \qquad (A.4f)$$

(The open–source program Maxima has been used.)

Using (A.3) to obtain initial values, we integrate (A.2a) towards $y = 0$. We find that as $y \to 0$, z diverges to $\pm\infty$ according as c is less than or greater than a critical value c'. As $c \to c'$, this divergence is confined to a region of decreasing size near O. The numerical solution consequently overlaps the small–y asymptote

$$z = y + y^5 + 31y^9 + 2986y^{13} + O(y^{17}), \qquad (A.5)$$

as can be seen in figure 4.

We conclude that $1.12271749510877 < c' < 1.12271749510879$, so

$$\lim_{\hat{h}\to\infty} \frac{\mathrm{d}\hat{h}}{\mathrm{d}\hat{x}} = 3^{1/4}c'. \qquad (A.6)$$

Appendix B. Material properties

Table 3 gives the values of material properties used in this work. According to Cazabat (pers. communication, 2013.03.17), laboratory temperatures ranged from 21–23 °C. Calculations in the text are based on properties at 22 °C (295 K). The conclusions from figure 5 would not affected by fluctuations of a few Kelvin about the value of 295 K despite the sensitive dependence of ρ_s on temperature: though for HMDS at 298 K, ρ_s would be almost 16% higher than at 295 K, the value of the independent variable $\mathcal{D}^{1/3}$ in figure 5 would be altered by only about 5%.

Though measured values of D_v were used for the alkanes, those for the linear siloxanes in air are not available. Values given in the table were obtained using the first–order Chapman–Enskog relation (Chapman and Cowling 1970, equation 14.2.4) and the expressions given as correlation (ix) in Tee et al. (1966, table 3). For octane and nonane, I found this method to predict the published experimental values of D_v to within 2% at the experimental temperature of 295 K. (Discrepancies between prediction and experiment are, however, appreciable at temperatures higher than those occurring in the Guéna experiments; see figures 3 and 5 of Chae et al. 2011.)

For siloxanes, the Chapman–Enskog prediction has been tested for two systems closely related to the one of interest. Park et al. (1987) measured the diffusivity of the cyclic molecule octamethylcyclotetrasiloxane OMcTS in air at 298 K; their measured value agreed to within about 30% with the Chapman–Enskog prediction. They describe this discrepancy as being 'large'. Maczek and Edwards (1979, table 7) measured the diffusivity of both HMDS and OMTS in argon (rather than in air) at 343 K; for both systems, their experimental values agreed to within 4% with the Chapman–Enskog prediction. Together, those studies suggest that Chapman–Enskog theory is adequate for our purpose.

		nonane	octane	HMDS	OMTS
D_v	mm^2/s	5.4^a	6.0^a	5.5^b	4.4^b
γ	mN/m	23	23	15.8	16.6
η_l	mPa s	0.67	0.53	0.50	0.88
ρ_l	kg/m^3	720	700	760	820
p_s	kPa	0.420^c	1.53^c	4.66^d	0.415^e
M	kg/mol	0.1283	0.1142	0.1624	0.2365
ρ_s	kg/m^{3*}	0.022	0.071	0.31	0.040
A	zJ†	1^f	1^f	1^g	1^g

TABLE 3. Material properties at 295 K. *a*, Berezhnoi & Semenov (1997), Beverley et al. (1999, figure 6 and table 2); *b*, Chapman & Cowling (1970, eq.14.2.4) ; *c*, Carruth & Kobayashi (1973); *d*, Flaningam (1986); *e*, Lindley & Hershey (1990); *f*, Gee et al. (1989, fig.6), Levinson et al. (1993, fig.3); *g*, Valignat et al.(1993, fig.4), A.–M. Cazabat (pers. comm.), Israelachvili (1991, table 11.3); *, ideal gas law; † 1 zJ (zeptojoule)=10^{-21}J. No source is given for values on which there is wide agreement.

REFERENCES

BEREZHNOI A. N. & SEMENOV A. V. 1997. *Binary Diffusion Coefficients of Liquid Vapours in Gases.* Begell House

BEVERLEY K. J., CLINT J. H. & FLETCHER P. D. I. 1999. *Phys. Chem. Chem. Phys.* **1** 149–153.

BONN D., EGGERS J., INDEKEU J., MEUNIER J. & ROLLEY E. 2009. *Rev. Mod. Phys.* **81**, 739–806.

CARRUTH G. F. & KOBAYASHI R. 1973. *J. Chem. Eng. Data* **18** 115–126.

CAZABAT A. M. & GUÉNA G. 2010. *Soft Matter*, **6** 2591–2612 doi:10.1039/B924477H

CHAE K., ELVATI P. & VIOLI A. 2011. *J. Phys. Chem.* B **115** 500–506.

DEEGAN R. D., BAKAJIN O., DUPONT T. F., HUBER G., NAGEL S. R. & WITTEN T. A. 2000. *Phys. Rev.* E62 756–765.

DOUMENC F. & GUERRIER B. 2010. *Langmuir* **26** 13959–13967 doi:10.1021/la1018373

EGGERS J. & PISMEN L. M. 2010. *Phys. Fluids* **22** 112101 doi:10.1063/1.3491133.

FLANINGAM O. L. 1986. *J. Chem. Eng. Data* **31** 268–272.

GEE M. L., HEALY T. W. & WHITE L. R. 1989.*J.Colloid Interface Sci.* **131** 18–23.

GIBBS J. W. 1875. *Trans. Connecticut Acad.* **3** 108–248. (*Collected Works*, **1**, p.160.)

GUÉNA, G. 2007.*Discussions sur l'évaporation d'une gouttelette mouillante.* Thesis number tel-00292745 at 'tel.archives-ouvertes.fr'

GUÉNA, G., ALLANÇON P. & CAZABAT, A.–M. 2007a. *Colloids Surfaces A* **300** 307–314 doi:10.1016/j.colsurfa.2007.02.009

GUÉNA G., POULARD C. & CAZABAT, A.–M. 2007b. *J. Colloid Interface Sci.* **312** 164–171. doi:10.1016/j.jcis.2006.06.023

HERVET H. & deGENNES P.–G. 1984. *C. R. Acad. Sc.* **299** II 605.

ISRAELACHVILI, J. 1991. *Intermolecular and Surface Forces.* 2nd ed. Academic.

KELLY–ZION P. L., BATRA J. & PURSELL C. J. 2013. *Int. J. Heat Mass Transfer* **64** 278–285.

LANDAU L. D. & LIFSHITZ E. M. 1960. *Electrodynamics of Continuous Media.* Pergamon.

LEVINSON P., VALIGNAT M. P., FRAYSSE N., CAZABAT A. M. & HESLOT F. 1993. *Thin solid films* **234** 482–485.

LINDLEY D. D. & HERSHEY H. C. 1990. *Fluid Phase Equilibria* **55** 109–124.

MACZEK A. O. S. & EDWARDS C. J. C. 1979. Viscosity and binary diffusion coefficients of some gaseous hydrocarbons, fluorocarbons and siloxanes. In *Symposium on Transport Properties of Fluids and Fluid Mixtures* National Engineering Laboratory, East Kilbride, Glasgow.

MORRIS S. J. S. 2001. *J. Fluid Mech.* **432** 1–30.

NJANTE J.–P. 2012. *Diffusion–controlled evaporating completely wetting meniscus in a channel.* Ph.D. dissertation. University of California, Berkeley.

PARK T., RETTICH T. R., BATTINO R. & WILHELM E. 1987. *Mat. Chem. Phys.* **15** 397–410.

POULARD C., GUÉNA G., CAZABAT A.–M., BOUDAOUD A. & BEN AMAR M. 2005. *Langmuir* **21** 8226–8233.

THOMSON W. 1872. *Proc. R. Soc. Edinburgh* **7** 63–68.

TRUONG J. G. & WAYNER P. C. 1987. *J. Chem. Phys.* **87** 4180–4188.

VALIGNAT M. P., FRAYSSE N., CAZABAT A.–M., HESLOT F. & LEVINSON P. 1993. *Thin Solid Films* **234** 475–477.